CONTROL OF BEAM LOSSES IN THE FRONT END FOR THE NEUTRINO FACTORY

C. T. Rogers, Rutherford Appleton Laboratory, STFC, Didcot, UK
D. Neuffer, Fermilab, Batavia, IL, USA
P. Snopok* Illinois Institute of Technology, Chicago, IL, USA; Fermilab, Batavia, IL, USA

Abstract

In the Neutrino Factory and Muon Collider, muons are produced by firing high energy protons onto a target to produce pions. The pions decay to muons which are then accelerated. This method of pion production results in significant background from protons and electrons, which may result in heat deposition on superconducting materials and activation of the machine preventing manual handling. In this paper we discuss the design of a secondary particle handling system. The system comprises a solenoidal chicane that filters high momentum particles, followed by a proton absorber that reduces the energy of all particles, resulting in the rejection of low energy protons that pass through the solenoid chicane. We detail the design and optimisation of the system and its integration with the rest of the muon front end.

HIGH POWER MUON ACCELERATORS

In the proposed Neutrino Factory [**?**] facility, a multi-megawatt proton beam is fired onto a target to produce pions. The pions are captured in a high field solenoid that tapers to a 1–2 T constant field solenoid. Pions and their decay products, the muons, are allowed to drift longitudinally in this constant field solenoid and subsequently a variable frequency RF system is used to bunch and then phase rotate the muons. Muons are subsequently passed into an alternating focussing ionisation cooling system before acceleration to high energy. The Muon Collider facility has a similar capture system, although the proposed ionisation cooling system is considerably more extensive in order to reach the very low emittances required for a high luminosity collider.

In this paper, we examine the effect of undesirable secondary particles exiting the target region and passing through the subsequent muon capture systems. Hadronic pollutants in the beam tend to cause activation of accelerator components, preventing hands-on maintenance of the machine. This would lead to additional construction and operation costs and is highly undesirable. Leptonic pollutants in the beam cause less activation of accelerator components but are still undesirable due to the increased heat load that may be placed on superconducting components.

* psnopok@iit.edu

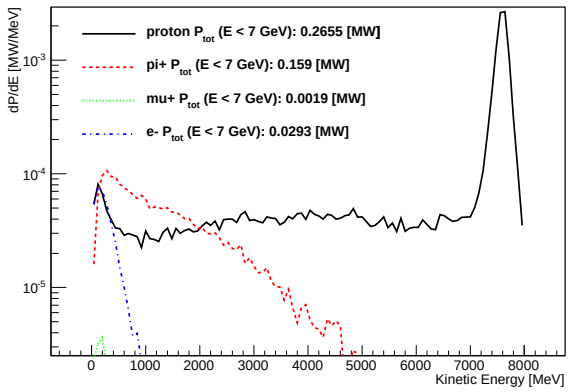

Figure 1: Power distribution of particles leaving the target. The peak at 8 GeV arises from primary protons travelling to the beam dump. Other particles are produced in the target resulting in significant beam impurities travelling into the front end system..

SECONDARY PARTICLE CONTAMINATION

The beam arising from the target is primarily made up of four constituent particles: protons; neutrons; pions and electrons. Additionally some muons, kaons and other particles may be present in the beamline. The muon capture system collects muons of both species in a momentum range roughly 100–400 MeV/c, while all other particles are considered contaminants that contribute only to uncontrolled losses in the later system. The relative composition of charged particles in the beamline is shown in Figure 1.

- Protons are the main contaminant. The peak at 8 GeV are primary protons that are lost in the target system, but there is a spectrum of secondary protons right from the lowest energies to the highest that are captured and transported.
- Pions are produced at energies up to about 5 GeV. Pions in the few-hundred MeV energy range contribute to the muon yield of the system, but other pions only contribute to uncontrolled losses.
- Electrons are produced at energies up to about 0.6 GeV. An additional high energy electron yield is expected arising from pion decay.

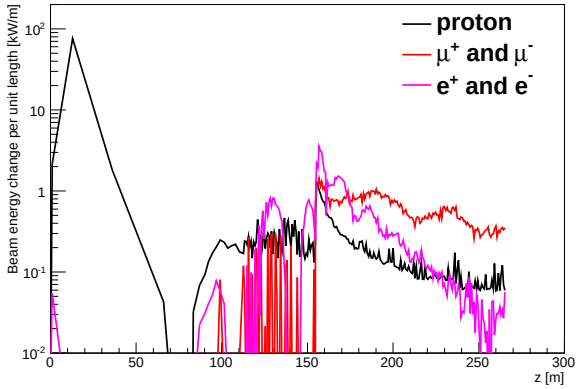

Figure 2: Total energy change of different particle species in the muon front end in the absence of a particle selection system, including gains and losses due to RF.

The effect of these contaminants can be seen in Figure 3. Losses are concentrated around the start of the ionisation cooling channel where the magnetic lattice produces large transverse losses and the presence of Lithium Hydride absorbers for ionisation cooling takes energy from electrons and protons. Losses are 100 W/m throughout the length of the front end and peak at several kW/m at the start of the cooling channel. Such high losses would certainly prevent hands on maintenance throughout the entire cooling channel, may cause radiation damage to equipment and quenching of superconducting magnets. Further contamination of critical components in the acceleration system is likely such as septa and injection/extraction systems.

Two components are foreseen for a particle selection scheme: a chicane to remove high momentum particles from the beam; and a Beryllium plug that reduces momentum of all particles in the beam, resulting in the loss of low momentum protons.

CHICANE DESIGN

The design of a chicane system for the muon front end is not trivial. Other authors have considered combined function chicanes [**?**] [**?**]. The beam emittance is such that it is highly challenging to get good transmission over the desired range of momenta using such a chicane. Both the Neutrino Factory and Muon Collider chicanes capture both positive and negative muon species, and any chicane system would be required to do the same. This may be possible with a multipole magnet, but would make any design more difficult.

Owing to these difficulties, a stellarator-type solenoidal chicane is foreseen as an alternative. Solenoidal chicanes induce a vertical dispersion in the beam, resulting in symmetric transmission between of both particle charges. Matching from the constant solenoid field of the front end to the bent solenoid field should be relatively easy. The main problem with this sort of lattice is that it is not possible to make an open midplane solenoid. Either very high radius superconducting coils with significant shielding or normal conducting coils exposed to beam power in the hundred kW range are required. Clearly these components would become active and it is expected that they would be treated as part of the remote handling facility in the target area.

The bent solenoid system that will be used for momentum collimation has its conceptual roots in the fields used to magnetically confined plasmas for nuclear fusion. The transport of particles by such a device is well known, although due to the nature of the problem, plasma confinement is generally treated statistically. In this paper the transport equations are calculated using a perturbative approach more conventional to accelerator physics where the paraxial approximation is valid. First the magnetic field is derived and this is used to calculate a reference orbit directly from the Lorentz force law. Then a Hamiltonian is generated and an infinitessimal transfer map is derived.

For this paper, the s coordinate is considered to be parallel to the coil axis, y is the vertical direction out of the chicane plane, ρ is the horizontal direction relative to the centre of the chicane curvature perpendicular to y and ρ and x is the horizontal direction from the coil axis parallel to ρ.

Magnetic Field in a Constant Radius Constant Field Bent Solenoid

The magnetic field in a bent solenoid is assumed to have only a radial dependence, such that it can be written as

$$\vec{B}_{bs} = f(\rho)\vec{s} \tag{1}$$

From Maxwell's equations, in the absence of current sources

$$\begin{aligned}\vec{\nabla}\times\vec{B} &= (\frac{1}{\rho}\partial_s B_y - \partial_y B_s)\vec{\rho} + \\ &\quad (\partial_y B_\rho - \partial_\rho B_y)\vec{s} + \\ &\quad \frac{1}{\rho}(\partial_\rho \rho B_s - \partial_s B_\rho)\vec{y} = 0.\end{aligned}$$

Substituting for $\vec{B}_{bs}$ gives

$$\partial_\rho \rho f(\rho) = 0 \tag{2}$$

which has the solution

$$f(\rho) = \frac{b_0}{\rho} = \frac{b_s\rho_0}{\rho}. \tag{3}$$

Here b_s is the magnetic field strength on the reference orbit at radius ρ_0.

Helical Motion

In the presence of a field of this nature, some particles can be shown to travel in a helix. Starting from the Lorentz equations,

$$\vec{F} = \frac{d\vec{p}}{dt} = q\vec{v}\times\vec{B} \tag{4}$$

it is possible to derive the criterion for helical motion. Assume no radial velocity, so that

$$\vec{v} = c\frac{p_y\vec{y} + p_s\vec{s}}{E} \tag{5}$$

with speed of light c. Then if the particle is travelling at radius ρ

$$\vec{F} = qc\frac{p_y b_0}{E\rho} \tag{6}$$

For circular or helical motion, with constant energy,

$$\vec{F} = m\gamma\rho\omega^2 = \frac{m\gamma\beta_s^2c^2}{\rho} = \frac{c^2p_s^2}{Er_0}. \tag{7}$$

By equating the two expressions for $\vec{F}$

$$\frac{c^2p_s^2}{E\rho} = qc\frac{p_y b_0}{E\rho}. \tag{8}$$

Then if

$$p_y = \frac{qp_s^2}{b_0} \tag{9}$$

particle motion will be on a helix. It should be noted that this motion is independent of the radius.

Vector Potential

The vector potential for the field can be found using the defining formula

$$\vec{B} = \nabla \times \vec{A} = \frac{b_0}{\rho}\vec{s} \tag{10}$$

Expanding the curl,

$$\begin{aligned}
\partial_y A_\rho - \partial_\rho A_y &= \frac{b_0}{\rho} && (11)\\
\partial_s A_y - \rho\partial_\rho A_y &= 0 && (12)\\
\partial_\rho \rho A_s - \partial_s A_\rho &= 0 && (13)
\end{aligned}$$

The gauge is chosen by comparison with the straight solenoid case,

$$\begin{aligned}
A_\rho &= b_s y\frac{\rho_0}{\rho} - \frac{b_s y}{2} && (14)\\
A_s &= 0 && (15)\\
A_y &= -b_s\frac{\rho - \rho_0}{2} && (16)
\end{aligned}$$

Near to the reference radius, with $\rho = \rho_0 + x$,

$$\begin{aligned}
A_x &= b_s y\frac{\rho_0}{\rho_0 + x} - \frac{b_s y}{2} && (17)\\
&= b_s y\sum_{i=0}^{i=\infty}\left(-\frac{x}{\rho_0}\right)^i - \frac{b_s y}{2} && (18)\\
&= b_s y\sum_{i=1}^{i=\infty}\left(-\frac{x}{\rho_0}\right)^i + \frac{b_s y}{2} && (19)\\
A_s &= 0 && (20)\\
A_y &= -\frac{b_s x}{2}. && (21)
\end{aligned}$$

It can be seen that as the radius of curvature tends to ∞, the field tends to a conventional solenoid field.

Hamiltonian

In order to study the motion of a particle beam, it is typical in accelerator physics to consider some perturbation of a reference orbit. Particles in the beam are considered to have small deviations from the reference trajectory, and the beam is said to be paraxial. In the bent solenoid discussed here, deviations are considered for particle trajectories near to the helical path discussed above.

The Hamiltonian in a curved coordinate system with radius of curvature ρ_0 is given by [**?**]

$$H = -(1+\frac{x}{\rho_0})(p^2-(P_x-qA_x)^2-(P_y-qA_y)^2)^{1/2}-qA_s \tag{22}$$

where P_i are the canonical momentum coordinates for the corresponding position variable i, related to the kinetic momenta by $p_i = P_i - qA_i$, and A_i are the magnetic vector potential magnitudes. In a pure magnetic field p is constant.

Taking a series expansion of the square root term in the Hamiltonian

$$\begin{aligned}
H &= -(1+\frac{x}{\rho_0})p(1 - && (23)\\
&\quad \frac{1}{2p^2}(p_x^2 - A_x^2 + 2p_xA_x - p_y^2 - A_y^2 + 2p_yA_y) && (24)\\
&\quad \frac{1}{8p^4}(p_x^2 - A_x^2 + 2p_xA_x - p_y^2 - A_y^2 + 2p_yA_y)^2 && (25)\\
&\quad \ldots) && (26)
\end{aligned}$$

or expressing as powers in the phase space coordinates

$$\begin{aligned}
H &= -(1+\frac{x}{\rho_0})p(1 - && (27)\\
&\quad \frac{1}{2p^2}(p_x^2 - A_x^2 + 2p_xA_x - p_y^2 - A_y^2 + 2p_yA_y) && (28)\\
&\quad \frac{1}{8p^4}(p_x^2 - A_x^2 + 2p_xA_x - p_y^2 - A_y^2 + 2p_yA_y)^2 && (29)\\
&\quad \ldots) && (30)
\end{aligned}$$

Chicane Momentum Collimation

The primary design criterion for the chicane is that it is as achromatic as possible. The chicanes explored in this paper have sufficiently weak bending that the transverse distribution is not significantly perturbed and only transverse-longitudinal correlations are significant.

The chicane was implemented in the G4MICE [**?**] tracking code as a series of individual coils and various parameters were varied to study the effect on the reference trajectory. In Figure **??** the transverse amplitude of particles of different momenta is plotted as a function of the bending angle per coil of the chicane. As the bending angle per coil was increased, the current was also increased to keep the overall magnetic field constant.

It can be observed that any dispersion in the lattice is well suppressed except in certain regions where resonance-type behaviour is observed. This behaviour appears to be quite independent of the actual coil geometry. The amplitude growth is not too significant for an appropriate choice

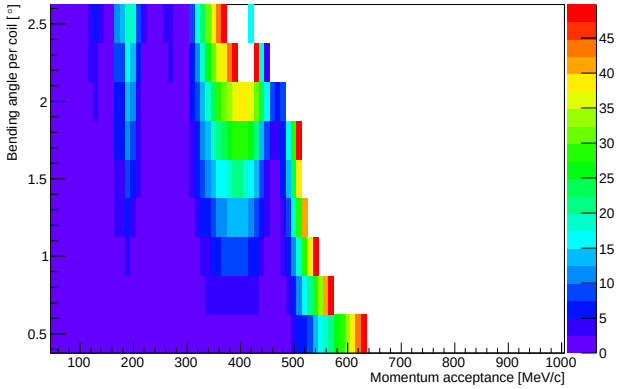

Figure 3: Change in particle amplitude upon traversing the chicane, for particles of varying momenta and chicanes of different bending angle.

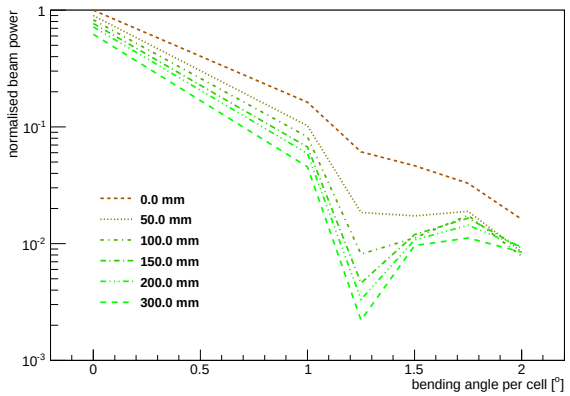

Figure 4: Total beam power of protons passing through the particle selection system, normalised to the case where particle selection system is in place.

of parameters and a very good momentum cut-off can be observed.

OVERALL SYSTEM DESIGN

The chicane system serves to remove high momentum particles from the system. The addition of a Beryllium plug after the proton absorber serves to lower the overall energy of particles in the system. This has a more significant effect on the protons that pass the chicane, stopping almost all of them, while leaving most muons in the beam. In figures 4 and 5 the proton beam power and good muon yield for the entire front end system is shown. Increasing thickness and increasing angle reduce the good muon yield slightly, while producing a dramatic reduction in the proton beam power escaping the system, with an acceptable compromise between reduced muon yield and proton absorbtion being the 100 mm, 1.25° point.

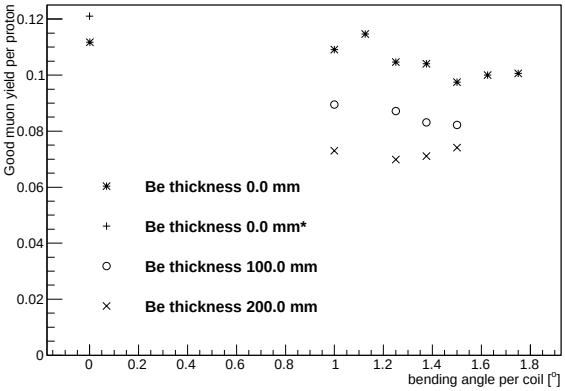

Figure 5: Number of good muons reaching the end of the muon front end cooling channel for various chicane angles and Be plug thicknesses. Note that for the 0 thickness, 0 angle case, two muon yields are listed; the '+' point is for an idealised lattice simulation, while the '∗' point and all other points are for a more realistic coil geometry.

FRONT END SIMULATIONS WITH CHICANE

When the chicane and absorber are added to the front end, the RF matching conditions for the buncher and phase-energy are shifted from the baseline conditions. In the chicane, the time-energy relationship is changed, requiring an increase in the drift by ≈1 m. The major change is imposed by the absorber, where the energy distribution is shifted to lower energies, see Fig. 6. The bunching is rematched by tracking the energy change in reference particles.

Two reference particles are set at the production target. The first is at 270 MeV/c and the second at 185 MeV/c. The time difference between these particles is tracked through the drift into the buncher and rotator to set the frequencies of the rf cavities. At z=29 m the beam and the reference particles pass through 10 cm Be absorbers, with the reference particle momenta reduced to 237 and 144 MeV/c, respectively. The drift to the buncher and rotator increases the distance between the particles $(\Delta c\tau)$ and the RF frequencies in the buncher are set by requiring that distance is 10 RF wavelengths ($\lambda_{rf} = (\Delta c\tau)/10$). The RF frequency decreases from ≈320 to ≈235 MHz over the buncher over the 33m length, as $\Delta c\tau$ increases. Following the buncher the beam and reference particles pass through the rotator where the RF wavelength difference is increased to 10.04, and the second reference particle accelerates while the first remains nearly stationary, while RF frequencies decrease from 232 for 202 MHz over the 42 m length. The beam is then matched to ≈230 MeV/c bunches at 201.25 MHz.

After rematching the drift section of the front end is increased by ≈5 m. The net number of muons that propagate through the system and arrive in the acceptance for accelerated muons is reduced by ≈10%. The background of beam propagating down the channel that is unmatched is reduced

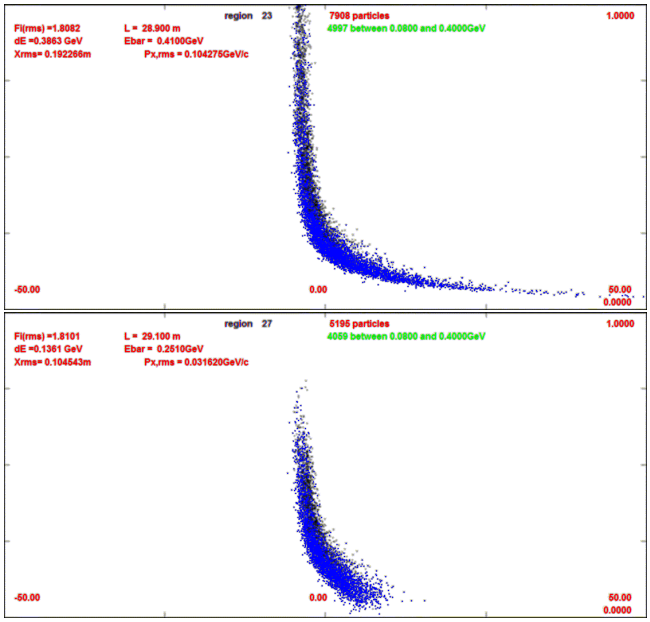

Figure 6: Phase–momenta distributions of the beam before and after the 10 cm Be absorber. Vertical scale 0 to 600 MeV/c; horizontal is $c\tau$ (-30 to 50 m).

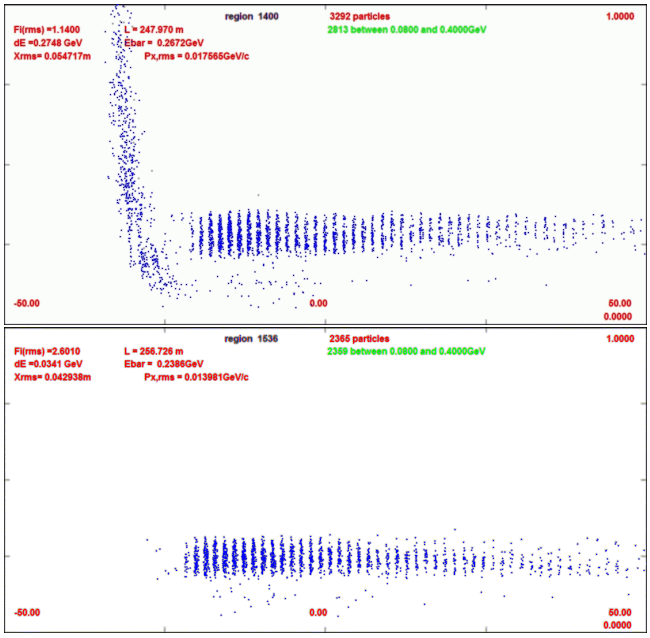

Figure 7: Phase–momenta distributions of simulated μ beam at the end of the cooling channel. Vertical scale 0 to 1000 MeV/c; horizontal is $c\tau$ (-50 to 50 m). First graph is without chicane/absorber; second is with chicane/absorber.

by much larger factors. The "pre-flash" of μ's from unmatched high energy μ's is eliminated.

The chicane removes high energy muons, which would continue down the cooling channel but not be properly phased for cooling. They would arrive at the end as a pre-flash of unmatched beam that would not be phased for acceleration and capture. The chicane/absorber beam is more background-free, see Fig. 7.

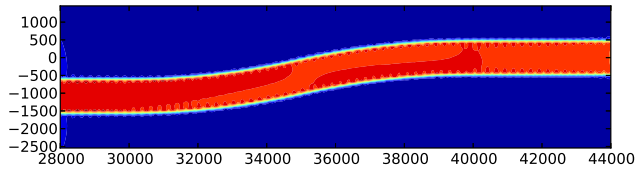

Figure 8: Magnetic field in the chicane, chicane angle 12.5 degrees.

MARS ENERGY DEPOSITION STUDY

The system as simulated in MARS [...] starts at the end of the target/capture region, 30 meters downstream from the muon target. The initial distribution of particles is an outcome of the target simulation by Nicholas Souchlas [...]. Part of the baseline front end drift channel lattice is replaced by a single chicane, nominally 12.5° each direction (other values of the chicane angle are considered as well). Field maps for MARS simulations are generated by G4beamline [...], the coil geometry is preserved for energy deposition calculations. Coils have inner radius of 43 cm, outer radius of 53 cm, length of 18 cm, with on-axis field of 1.5 T throughout the channel, see Fig. 8. Coils are superconducting, standard MARS material SCON consisting of 90% superconductor (60% Cu and 40% NbTi) and 10% kapton ($C_{22}H_{10}N_2O_5$) is used for simulations. The proton absorber is a 10 cm Be disk of outer radius of 42.9 cm.

No chicane, no absorber

The case of a straight drift channel with no chicane and no absorber is used as a reference. In this case the peak total deposited power density (DPD) in the coils is 0.148 mW/g (a common 0.15 mW/g limit for superconducting coils is not exceeded), see Fig. 9. In terms of peak linear power density for the geometry described above that corresponds to 399.128 W/m for Cu coils or 311.818 W/m for superconducting coils. That is significantly larger than the typical 1 W/m limit for hands-on operation; however, average linear power density is much less, 34.087 W/m for Cu coils and 26.631 W/m for superconducting coils.

At the same time, 100% of both high and low energy protons will propagate to the end of the drift channel, and the proton absorber alone will not be sufficient. The power of the muon component of the beam at the downstream end of the drift section is 148.6% of the initial value for μ^+ and 146.4% for μ^- for muons of all energies, or 135.8% and 132.9% for momenta in $[100, 400]$ MeV/c range.

Varying angle chicane, Be proton absorber

High energy protons are not bent by the chicane, they go directly through some of the coils which therefore have to be made normal conducting, and into the beam dump. Low

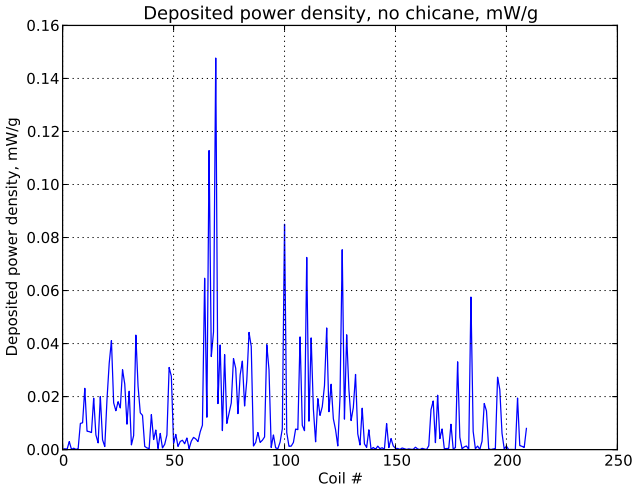

Figure 9: Deposited power density, drift channel, no chicane.

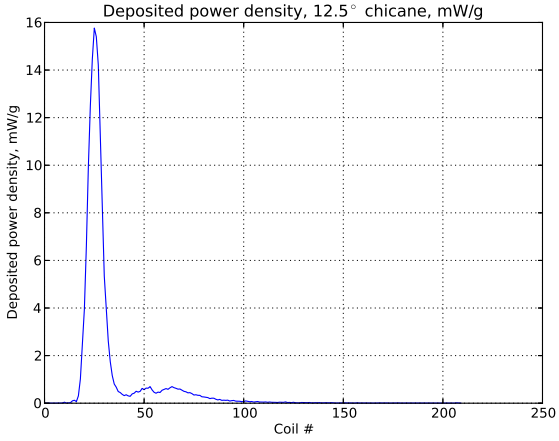

Figure 10: Deposited power density, drift channel, nominal 12.5° chicane.

energy protons traverse the chicane and are stopped in the Be proton absorber that has little effect on muons.

Basic radiation limit of 0.15 mW/g is exceeded in coils #18 through #89; however, it could be reasonably reduced by providing extra shielding in coils #40 and up, so only coils #18–39 need to be replaced by warm normal conducting ones. Deposited power density (DPD) peaks at coil #26 at 15.765 mW/g with a significantly longer right tail in the DPD distribution due to the contribution from protons of lower energies, see Fig. 10. That translates into 42.602 kW/m for Cu coils or 33.282 kW/m for superconducting coils. Proton absorber DPD is 292.25 mW/g or 312.262 kW/m.

Proton, μ^+ and μ^- beam power ratios (compared to the initial distribution at 30 m downstream of the target) are summarized in Table 1 for various chicane angles.

Table 1: Beam power ratios for protons and muons before and after the chicane/absorber for various chicane angles.

Chicane angle [deg]	p [%]	μ^+ [%]	μ^- [%]
no momentum cut			
0.75	33.3/9.4	91.0/75.5	93.8/75.8
1.00	22.7/2.7	77.3/62.1	81.8/64.5
1.25	18.5/1.0	70.1/55.5	74.7/57.7
1.50	15.1/0.3	62.0/48.5	68.5/52.3
1.75	12.7/0.2	55.9/43.2	63.0/47.4
Momentum cut $p \in [100, 400]$ MeV/c			
0.75	70.8/25.3	112.9/96.7	113.8/95.6
1.00	37.4/5.8	113.1/95.2	110.4/91.6
1.25	18.1/0.8	112.7/92.9	108.2/87.1
1.50	6.2/0.1	104.6/84.3	103.5/80.9
1.75	1.7/0.1	96.9/74.1	96.7/72.9

CONCLUSIONS

Summary of work. Engineering challenges (normal conducting vs superconducting).

BIBLIOGRAPHY